Appendix S1 Supplementary information

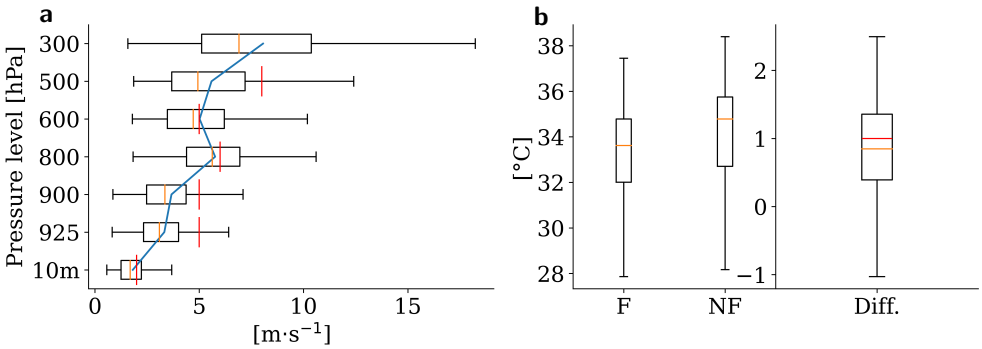

Figure S1. **a,** Box and whisker diagrams of ERA-5 wind in m $s^{-}1$ over the Rondônia domain denoting the 10, 25, 75 and 90th percentiles for the August-October 2019 -2022 period. Yellow bars denote the median and blue curve denotes the average. **b,** Same as **a** but for skin temperate in °C. Left panels shows average skin temperature at 11:00LT between the forest (F) and non-forest (NF; boundary region excluded) and the panel on the right shows their difference. Red bars denote the conditioning thresholds.

Table S1: WRFV4.2 Configuration

Grids	HE0.5	HE1	HE2	HP2	HE5	HE10
dx, dy ($nx \times ny$)	0.5km (1200 × 1200)	1km (600×600)	2km (300×300)	2km (300×300)	5km (120×120)	10km (60×60)
dt	3s	5s	10s	10s	20s	20s
Turbulence	1.5OTKE	YSU	YSU	YSU	YSU	YSU
Convection scheme	-	-	-	KF [69]	-	-
dz	50-16000m (nz = 40)					
Microphysics	Single-Moment 6-Class Microphysics [67]					
Land surface	Noah Land Surface Model [75]					
Radiation	Rapid Radiative Transfer Model (RRTMG; [76])					
Thermal forcing	Sunrise: 6:00 LST, solar maximum: 12:00 LST, sunset: 18:00 LST					
Bowen ratio (β)	'Dry' patch: 1.55, 'Wet' patch: 0.45					

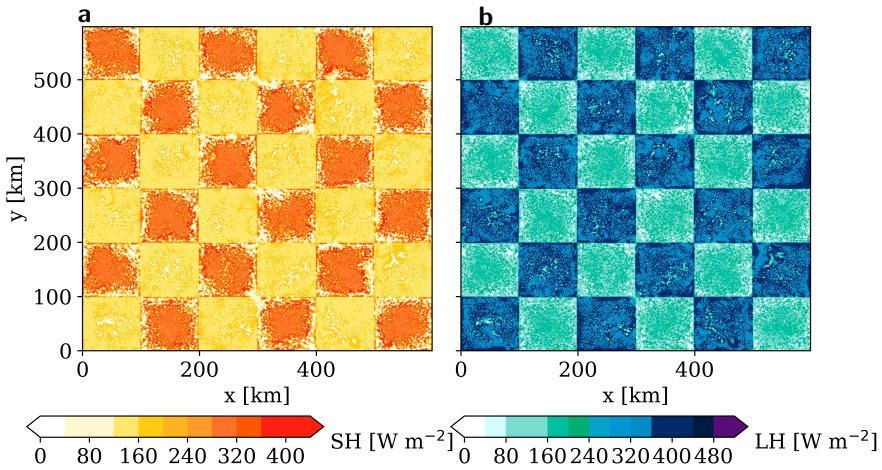

Figure S2. **Response of surface heat fluxes to the imposed checkerboard pattern of wet/dry soil moisture states.** Sensible **a,** and latent heat flux **b,** in W m^2 for the full domain of the HE1 simulation at 11:00 LT.

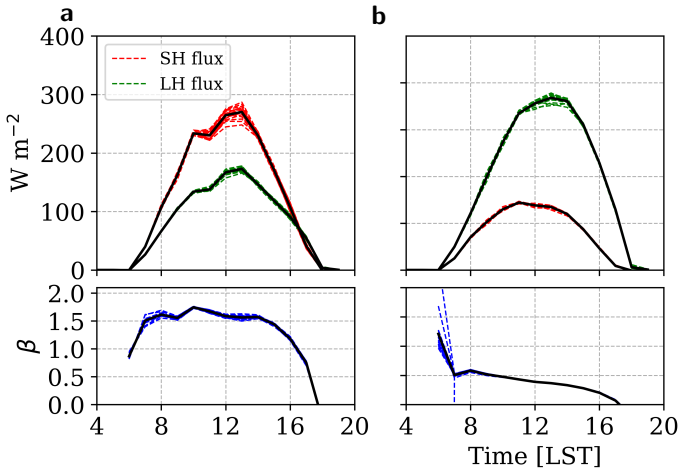

Figure S3. **Example of the diurnal cycle of surface heat fluxes for the HE1 simulation.** Patched averaged sensible (red dashed) and latent heat flux (green dashed) in W m^2 shown in the top panels for **a,** dry patches and **b,** wet patches. Bowen ratio (β) is shown in the bottom panel. Black lines indicate the average value across all patches.

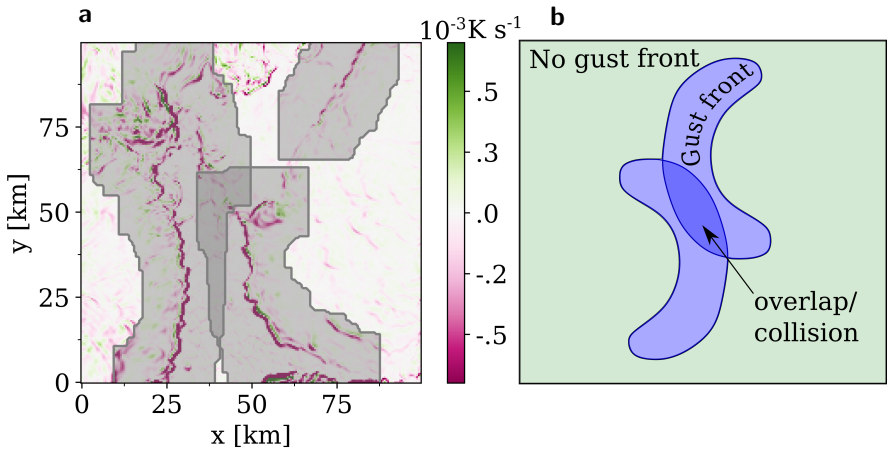

Figure S4. **a,** Snapshot of horizontal advection of surface virtual temperature (shading, K s^{-1}) at 18:15 LST. Gust front boundaries are shown in light grey shading, with overlap in darker grey shading. Saturated magenta regions correspond to gust fronts associated with cold pools. **b,** Schematic illustration showing the grid classification into gust front objects, collision objects where gusts overlap, and no gust front.

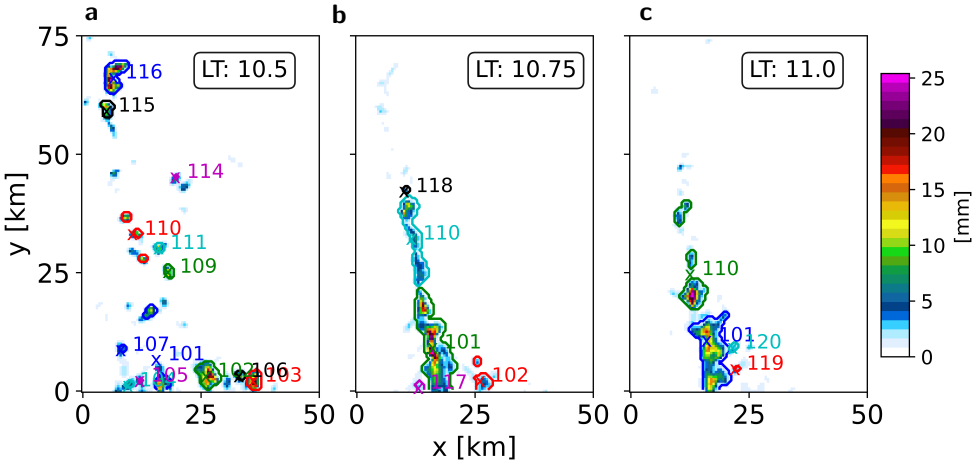

Figure S5. **Example of merging and splitting cells in the HE0.5 WRF simulation**. Shows 15-minute accumulated precipitation (shaded; mm) with contours denoting storm objects identified by the storm tracking procedure at **a,** 10.25 LT, **b,** 10.5 LT and **c,** 11 LT. 'x' denotes the centroid of the identified storm objects and numbers denote their unique identifiers.

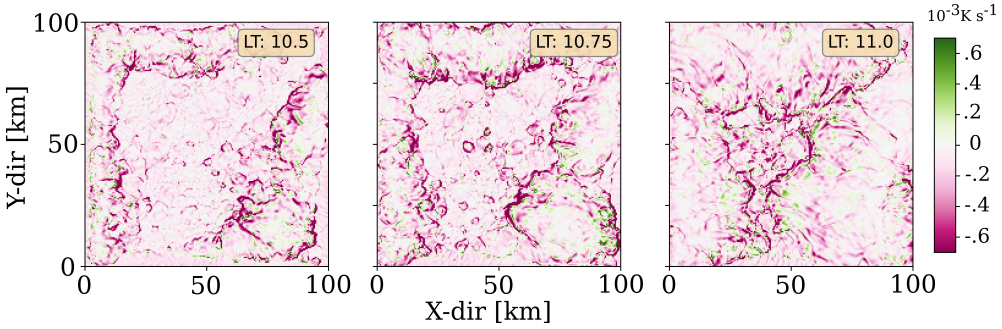

Figure S6. Snapshots of WRF horizontal advection of surface virtual temperature (shading, K s^{-1}) at 10:30, 10:45 and 11:00 LST. Saturated magenta regions correspond to gust fronts associated with cold pools.

Figure S6 shows a top down view of CP gust fronts (saturated magenta regions in arc shapes) triggered by thunderstorms along the edge of a dry SM moisture patch at 10:30 LT in the HE1 simulation. By 10:45 the CPs coalesce to form larger, more organized fronts, moving preferentially toward the centre of the dry patch in the direction of the convex side the arc, where they converge by 11:00 LT.

To elaborate more on the previous figure, figure S7 showcases the vertical profile along the zonal direction at y = 50km of modelled processes that are key to understanding the enhancement of thunderstorms over significant LULLC regions. At 10:00 LT a 2K temperature difference develops between the wet and dry SM patches (see green dashed curves in the bottom panels; Fig. S7a and b). This temperature differential is responsible for the shallow circulation, below 1.5km height, that develops along the boundary of the wet/dry SM patches, seen by the black contours on the vertical dashed line. Wind is moving from the wet to dry SM patch at a maximum velocity of approximately 2 m s^{-1} near the surface on the dry side of the patch (Fig. S7a and b). Figure S7b also shows cooler air (and moist - not shown) advected into the dry patch, associated with the thermal circulation. The circulation is also present on the opposing side of the dry patch near x = 100km.

Water mixing ratio indicates moist convective cell initiation across the dry patch, with more organized thunderstorms triggered at the breeze fronts (Fig. S7a). [19] showed that in such a scenario, CP outflow from thunderstorms merges with the breeze front, resulting in the front to accelerate in the direction of the warmer air. The result of this processes is shown in figure S7c and d, where opposing circulations associated with cooler air converges near the center of the patch, from which a large thunderstorm complex emerges (Fig. S7c).

It is also important to note that there is no outflow that similarly moves into the wet patch, indicating that the thermal breeze, and thus land surface, imposes a preferred direction of movement for the convective CP outflow. Later during the day, although not shown, large organized convective CPs generated from the thunderstorm complex over the centre of the dry patch does eventually migrate into the wet patches. These CP's occasionally collide over the wet patches, triggering thunderstorms that are distinctly organized in patterns that depend on the location of the dry boxes the CP's migrate from.

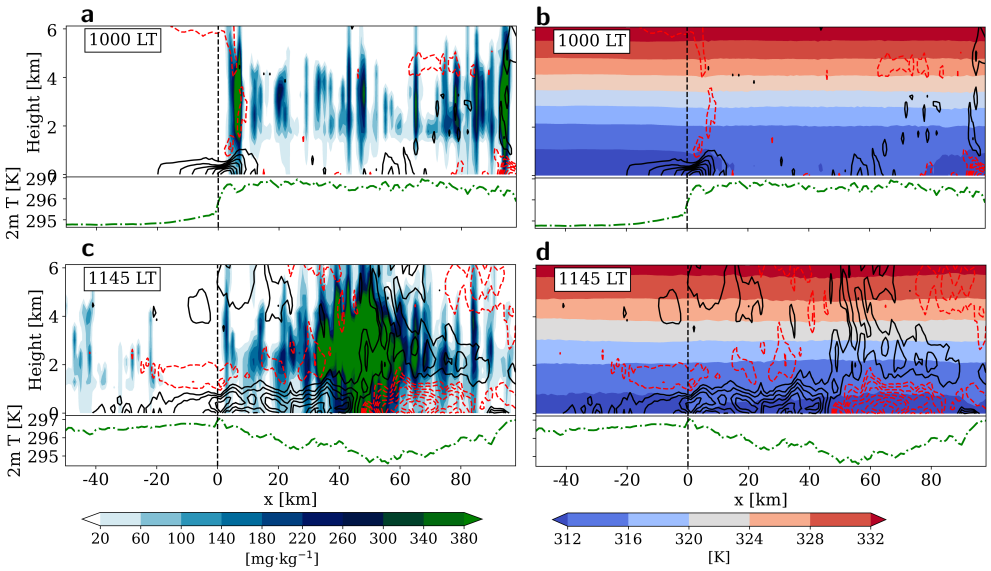

Figure S7. Vertical cross sections averaged across all dry and wet SM patch pairs for the HE1 simulation of **a,** 10:00 LST zonal wind component (increments of 0.2 m s^{-1}; top panel) contoured (black for positive, red for negative), water mixing ratio (mg kg^{-1}; shaded) and 2m temperature (K; bottom panel), **b,** same as **a** but with potential temperature (K) shaded. **c,** Same as **a** but at 11:45 LST and **d,** same as **b** but at 11:45 LST. The wet (dry) patch is located to the left (right) of the vertical dashed line at x = 0.

Precipitation initiates along the edges and corners of the dry SM patches (Fig. S8a—c panels 1 and 2) and, as one would expect, the contribution to the total rainfall at this time is dominated by triggers outside of gust front and CP collisions (green dotted line). However, toward the centre of the dry patch (30 to 50 km into the patch) in the HE2 simulation, rainfall is dominated by thunderstorms triggered from gust fronts (red dashed line in Fig. S8c panel 3). This is in contrast to the HE05 and HE1 simulation where the time series for this region show that the peak in precipitation coincides with CP collision triggered thunderstorms (blue lines, panel 3 Fig. S8a and b) as the primary source of precipitation, followed closely by gust front triggered precipitation (red dashed lines). It is also interesting to note that the second peak in precipitation in the centre of the HE05 patch (panel 3), which is not present in the HE1 or HE2 simulation, occurs at the same time when there is a sharp increase in CP collision derived precipitation, such that the precipitation contribution from CP collision triggered thunderstorms are close to 100%.

In figure S9 at the time of the first detected storms (t=0), taken from 3 days of the HE1 simulation, mean of the maximum vertical velocity at 1km model height is at a minimum. This minimum is due to criteria for detecting storms that are based on a precipitation threshold criteria, resulting in downdrafts detected at t=0. In all three simulations the minimum is consistent at about 1.5 m s^{-1}. All three simulations exhibit a jump in updraft velocity 30 to 45 minutes prior to the detection of the storms when the

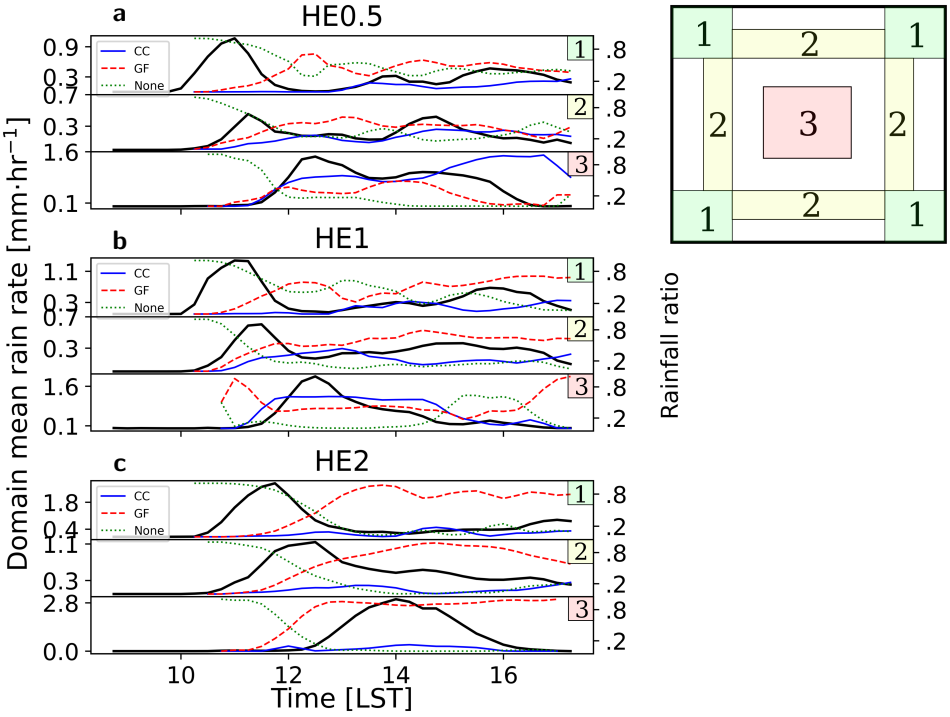

Figure S8. Time series of domain average rain rate (mm hr^{-1}; black line) and the respective contribution, as a ratio, to the total hourly rain by thunderstorms triggered by isolated gust fronts (red dash), colliding CPs (blue solid) and neither (green dotted). Rain rates are averaged over the domains demarcated in the top right panel by 1 = corners, 2 = sides and 3 = centre.

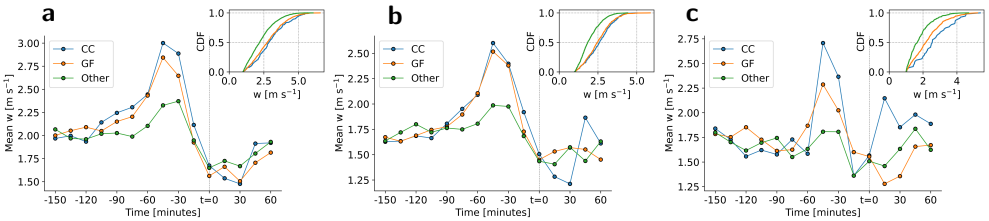

Figure S9. Time series of WRF simulation mean of maximum vertical velocity (w; m s^{-1}) at 1km height in a 1x1 grid point box around the centroid of initial storm object locations for **a,** HE05 simulation; blue curves denote CP collision triggered storms, red gust front triggered and green other. Grey vertical line denotes the time of initiation at t=0. Top right panel is the probability density function of max. w (¿ 1m s^{-1}) at the time of peak max. w. **b,** same as **a** but for the HE1 simulation and **c,** same as **a** but HE2.

storms initiate. While the updrafts from the CP collision and gust front triggered storms (blue and red curves) are stronger by 0.5 to 0.8m s^{-1} relative to the other storms (for all three simulations), the overall updraft speed is strongest in the HE05 simulation. The HE1 storms has about 1m s^{-1} weaker maximum updraft velocity compared to H05 storms, and the HE2 storms an average updraft velocity weaker by a factor of two compared to the H05 storms. This explains to a large degree why storms produce higher extreme (99th percentile) rainfall amounts, and larger storms at the extreme ends, in the HE05 and HE1 simulation compared to the HE2 simulation (*see* Fig. 6).

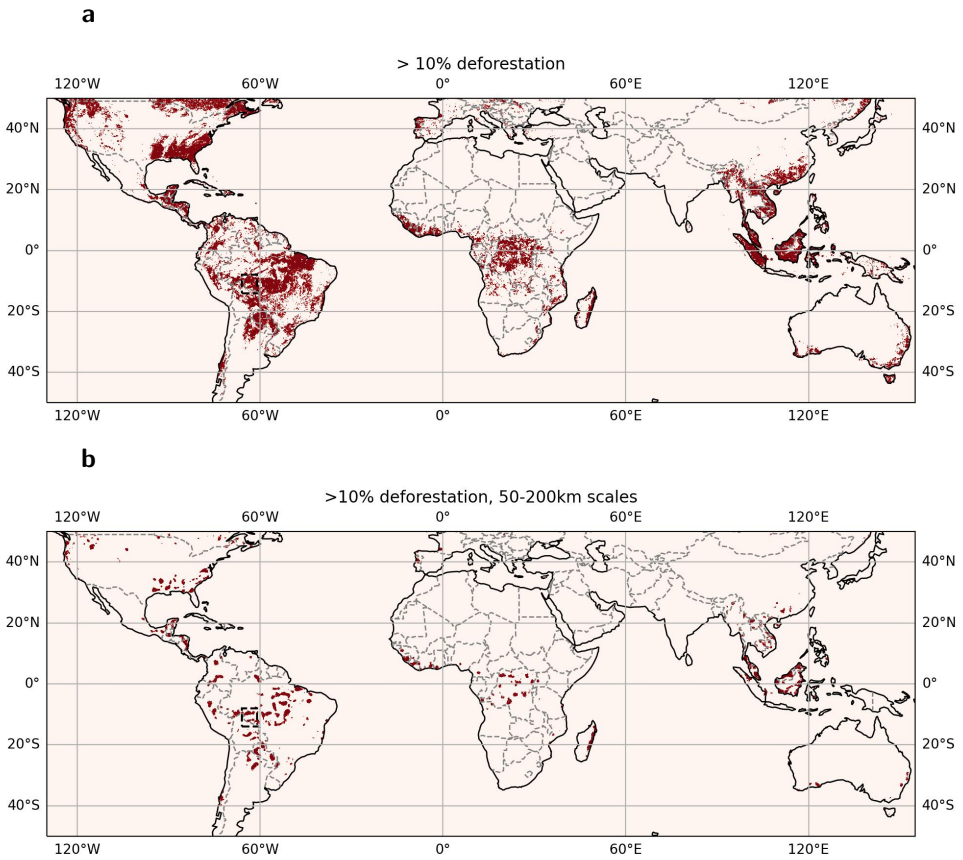

Figure S10. **Areas across the globe within potentially similar convective organization extremes.** HANSEN deforestation dataset re-gridded to 0.05 degrees, showing pixels with **a** >=10% deforestation since the year 2000 (considers change 2000-2022) and **b,** same as **a** but for >=10% deforestation scales of between 50-200km^2